



Amplification of compound hot-dry extremes and associated population exposure over East Africa

Brian Odhiambo Ayugi¹ · Charles Onyutha² · Kenny Thiam Choy Lim Kam Sian³ · Huanhuan Zhu³ · Hassen Babousmail³ · Eun-Sung Chung¹

Received: 13 March 2024 / Accepted: 28 August 2024
© The Author(s), under exclusive licence to Springer Nature B.V. 2024

Abstract

Quantifying the vulnerability of population to multi-faceted climate change impacts on human well-being remains an urgent task. Recently, weather and climate extremes have evolved into bivariate events that heighten climate risks in unexpected ways. To investigate the potential impacts of climate extremes, this study analyzes the frequency, magnitude, and severity of observed and future compound hot-dry extremes (CHDEs) over East Africa. The CHDE events were computed from the observed precipitation and maximum temperature data of the Climatic Research Unit gridded Timeseries version five (CRU TS4.05) and outputs of climate models of Coupled Model Intercomparison Project Phase 6 (CMIP6). In addition, this study quantifies the population exposure to CHDE events based on future population density datasets under two Shared Socioeconomic Pathways (SSPs). Using the 75th/90th and 25th/10th percentile of precipitation and temperature as threshold to define severe and moderate events, the results show that the East African region experienced multiple moderate and severe CHDE events during the last twenty years. Based on a weighted multi-model ensemble, projections indicate that under the SSP5-8.5 scenario, the frequency of moderate CHDE will double, and severe CHDE will be 1.6 times that of baseline (i.e., an increase of 60%). Strong evidence of an upward trajectory is noted after 2080 for both moderate and severe CHDE. Southern parts of Tanzania and northeastern Kenya are likely to be the most affected, with all models agreeing (signal-to-noise ratio, SNR > 1), indicating a likely higher magnitude of change during the mid- and far-future. Consequentially, population exposure to these impacts is projected to increase by up to 60% for moderate and severe CHDEs in parts of southern Tanzania. Attribution analysis highlights that climate change is the primary driver of CHDE exposure under the two emission pathways. The current study underscores the urgent need to reduce CO₂ emissions to prevent exceeding global warming thresholds and to develop regional adaptation measures.

Keywords Compound extremes · Climate change · CMIP6 GCMs · CRU · Precipitation · Maximum temperature

Extended author information available on the last page of the article

1 Introduction

Reports of the Intergovernmental Panel on Climate Change (IPCC) show that extreme weather and climate events, including extended megadroughts, flash floods, wildfires, and compound extremes, have been recorded in several regions of the world due to the net effect of human-caused global warming (IPCC et al. 2021). This has resulted in unprecedented destruction of infrastructure, colossal economic losses, deaths, and displacement of people from their homes. Recently, several studies have detected a general increase in the frequency, magnitude, and severity of compound extremes (events that occur concurrently), such as compound hot-dry extreme (CHDEs) in the context of global warming, threatening sustenance, water availability, and ecological systems (Hao et al. 2013; Aghakouchak et al. 2020; Pendergrass et al. 2020; Wu et al. 2021). CHDE, characterized by high air temperature (i.e., hot extremes) and low atmospheric humidity (i.e., dry extremes) often result in severe disasters such as flash droughts and heatwaves among others (Zhang et al. 2023). Improved knowledge of their variability, future evolution, and net effect on the human population is required for informed planning of adaptation measures against potential impacts across vulnerable regions such as sub-Saharan Africa.

Numerous studies have shown disproportionate impacts of compound extremes across various parts of the world under both historical and future climatic conditions (Zhang et al. 2021, 2022; Zhou et al. 2023; Ullah et al. 2023; Tabari and Willems 2023; Zhao et al. 2023). For example, Sun et al. (2023) reported a severe impact of compound heatwaves in Southeast Asia (SEA) that will affect the younger generation born in the 2010s compared to those born in the 1980s. The study noted that Indonesia would be the region most affected by compound extremes, thus calling for heat-stress adaptation strategies in such locations. Over Europe, a recent study (Dosio et al. 2023) reported that CHDEs would affect the region of the Iberian Peninsula at least twice every three years, and up to about 60% of the entire region is projected to be affected even under a low emission scenario. Zhang et al. (2022) noted that the large expanse of arid and semi-arid regions, such as the Sahara, Mediterranean, and parts of Central America, will experience the largest population exposure to compound extremes. The net effect of compound extremes was quantified in a recent study, with findings showing that up to about 119 million additional people globally will be affected by bivariate events (Tabari and Willem 2023). Such emerging studies highlight the urgent need to implement mitigation strategies to alleviate the impact of CHDEs on human society.

While the studies mentioned above have quantified the impact of CHDEs across various parts of the world, few studies have been conducted over the continent of Africa to estimate the observed or projected changes of CHDEs and their impact on vulnerable populations. Many existing studies that focus on the entire globe consider the African continent as a single averaged zone, thus, overlooking regional variations and specific vulnerabilities (Hao et al. 2020; Wu et al. 2021; Meng et al. 2022; Bevacqua et al. 2023). Currently, few regional studies have been conducted to characterize the spatiotemporal scales of compound events. For instance, in Africa, Camara et al. (2022) employed the Regional Climate Models version 4 (RegCM4) to characterize the changes in CHDE events along the Sahara Desert. The study established that restoration of the Sahara Desert could adversely affect the occurrences of CHDEs. Meanwhile, Obahoundje et al. (2023) examined the impact of changes in upper atmospheric layer aerosols on compound temperature and precipitation extremes over Africa using Coupled Model Inter-comparison Project phase five (CMIP5 GCMs). Findings include notable future changes

in both variables compared to the historical period. Similarly, employing downscaled models from the Coordinated Regional Climate Downscaling Experiment-Coordinated Output for Regional Evaluations (CORDEX-CORE), Weber et al. (2020) also noted a pronounced increase in the frequency of compound extremes, particularly under high CO₂ emission scenarios in Africa. These existing studies have pointed out some important findings that warrant further analysis to deepen our understanding of the potential impacts of emerging extremes on vulnerable populations and regions, such as the African continent.

Compared to other sub-regions in Africa, East Africa (EA) remains the most susceptible sub-region that continues to experience recurrent CHDE due to prolonged droughts and heatwave events (AghaKouchak 2020; Funk et al. 2023; Ayugi et al. 2022). A recent study by Muheki et al. (2024) reported that the region will experience an increase in the area affected by the compound extremes, with the strongest increase for joint heatwaves and wildfires (+940% by 2100 under the representative pathways concentration (RCP) 6.0 relative to the present day). Moreover, the study reported that in addition to heatwaves and wildfires, the region will experience an increase in compound river flood and heatwave events (>900% in the far-future). The recent unprecedented occurrence of eight consecutive drought episodes since late 2016, coupled with heatwaves, has affected millions of people, with an estimated aid cost exceeding 2 billion USD (Omondi and Lin. 2023; Haile et al. 2020; Funk et al. 2023). Moreover, projections show that the region will experience an increase in temperature, higher variability in rainfall, and shorter seasons (late onset and early withdrawal of rains) due to stronger Pacific Ocean Sea surface temperature (SST) and steeper Indian Ocean SST gradients (Funk et al. 2023). These factors collectively contribute to altering the region's weather and climate, underscoring the urgent need to quantify the anticipated climate change impact on the population and implement appropriate adaptation measures in response to observed and projected extreme events.

Consequently, to delineate the net effect and evolution of compound extremes over EA, which is the second most populous sub-region of the continent (~400 million persons) (Niang et al. 2014) and most vulnerable due to the dependency on rainfed agriculture for food security (Niang et al. 2014; Onyutha 2019), there is a need to quantify the recent observed and future changes in CHDE events. Existing studies have faced shortcomings, including using coarser resolution GCMs, uncertainty in model projections, and the lack of quantification of population exposure. While more recent studies have demonstrated the improved performance of the Coupled Model Intercomparison Project Phase Six (CMIP6) compared to its predecessors (Ayugi et al. 2021a, b; Zhu et al. 2021), it still contains persistent biases and challenges to accurately simulate extreme events (Akinsanola et al. 2021; Onyutha 2020), as well as uncertainties climate projections (Brunner et al. 2019). In response, scientists have made concerted efforts to minimize model spread to reduce overall uncertainty, employing methods such as bias correction or dynamical downscaling techniques (Brunner et al. 2019). Consequently, numerous recent studies have adopted various approaches that involve weighting models and selecting those with higher weights to better represent real uncertainty (e.g., Li et al. 2016; Sanderson et al. 2017; Zhu et al. 2023).

This study adopted a probabilistic approach to investigate the changes in CHDE over EA (Fig. S1), which has recently been experiencing recurrent extreme climate events (Ayugi et al. 2021a, b, 2023; Omondi and Lin. 2023). The study focused on the following gaps: (1) How has CHDE evolved over the EA in the recent past? (2) How will CHDE events change in the mid-future (2041 – 2060) and far-future (2081 – 2100) under varying climate scenarios? (3) How will CHDE events affect the population, and which region will most likely be affected? (4) What is the main driver of CHDE events over EA?

2 Study domain, climate variables and methodology

2.1 Study domain

The study focuses on the EA region, which is delineated by the geographical coordinates ranging from latitude 12°S and 5°N and longitude 28°E and 42°E (Fig. S1). The region is further sub-divided into two climatic zones following recommendations from the IPCC Working Group 2 (Irtubide et al. 2020). However, this study explores the changes in CHDEs across the entire region, considering changes in temperature and precipitation. For instance, the relationship between temperature and precipitation shows a negative correlation of up to -0.8 in western and southern areas, while the northeastern and coastal belt regions show a correlation coefficient above 0.4 (Fig. S2). Monthly shifts in geographical areas characterized by strong correlation between precipitation and temperature follows an analogy of the latitudinal migration of the Inter-Tropical Convergence Zone (ITCZ) (Onyutha 2021). Furthermore, the linear slope indicates a decrease in maximum temperature (-0.002 °C/decade), while precipitation shows an increasing trend of 0.731 mm/decade (Fig. S3). This suggests that warm (cold) temperatures coincide with fewer (heavy) precipitation events, resulting in warm/dry and cold/wet events as demonstrated in a previous study (Nicholson 2017) conducted considering EA during 1995–2014. Temporal increase in temperature was shown to coincide with the decrease in precipitation total across Africa where the study area is located considering 1901–2015 (Onyutha 2021).

2.2 Datasets

The study utilizes observed monthly global precipitation (pr) and maximum temperature (T_{\max}) datasets obtained from the Climatic Research Unit gridded Timeseries version five (CRU TS4.05; Harris et al. 2020). The datasets are employed to analyze CHDE over the EA region during the recent 20 years. The CRU datasets have a temporal monthly resolution spanning over 120 years and a 50 km by 50 km grid horizontal resolution over all land domains except Antarctica. These datasets are developed using an interpolation algorithm that utilizes angular-distance weighting for monthly climate anomalies sourced from vast networks of weather stations distributed globally (Harris et al. 2020). The quality of the gridded products is ensured through nearest-neighbor checks and a long-term historical record check to maintain consistency and reliability. Previous studies conducted over EA have confirmed the robust performance of CRU products (e.g., Ayugi et al. 2016; Ongoma and Chen. 2017).

Next, the study employs global climate models (GCMs) sourced from CMIP6 (Eyring et al. 2016) for daily pr and T_{\max} to estimate future changes in CHDE events. These datasets span from 1850 – 2100 with varying grid horizontal resolution. For consistency, the study selects twenty-one models (Table S1) that have the two scenarios representing the moderate and worst-case and the first variant (r1i1p1f1). The ensemble used represents the same initial and physical conditions, and as well as forcing. The historical period considered in the present study is 1995 – 2014, which follows the period used by the recent IPCC report working group 1 (IPPC et al. 2021). For future projections, the study uses models under the Shared Socioeconomic Pathways (SSP) scenarios, illustrating a sustainable approach to cap temperature rise to 2.5 °C (SSP2-4.5) or, in the worst-case scenario (SSP5-8.5), no policy implementation leading to a temperature rise exceeding 5 °C (O'Neill et al.

2017). The study explores future changes in CHDE under two future periods: mid-future (MF, 2041 – 2060) and far-future (FF, 2081 – 2100). Several studies conducted across the globe (Almazroui et al. 2020a, b; Deegala et al. 2023; Lu et al. 2022) and sub-regions of Africa (Nooni et al. 2023a) have utilized CMIP6 models, demonstrating the models' skill in representing the historical climate of the continent. Recent studies over EA have also shown the robust performance of the CMIP6 models compared to their predecessors (Song et al. 2021; Dioha et al. 2024; Ayugi et al. 2021a, b).

Lastly, the study uses population datasets from the Gridded Population of the World (GPWv3) datasets to examine the population exposure to CHDE over EA. Similar to the climate models, we obtain the projection datasets for grids based on SSP2 (sustainability pathways) and SSP5 (Anthropocene pathways) for 2010 – 2100. The population data for 2010 is used to represent the historical period, while projection datasets span from 2011 to 2100 under varying SSPs. More details regarding the products can be obtained from Jones and O'Neill (2016). Previous studies have employed demographic products to assess the risk of global climate change following single-hazard or compound extremes to populations (Ayugi et al. 2022; Tabari and Willems 2023).

For uniformity purposes, all the datasets used in this study are re-gridded to a common horizontal grid resolution of $1^\circ \times 1^\circ$ using a bilinear interpolation approach for observed and climate models.

2.3 Methods

2.3.1 Computation of CHDE events

To further explore spatial changes in CHDE events in EA, this study analyzes the spatial variance of bivariate event frequency that is likely to happen in future periods. The study uses monthly-accumulated pr and monthly-averaged T_{\max} to derive the moderate and severe CHDE on an annual scale, considering total occurrences for each month. Here, various quantiles are used following the benchmark procedure previously employed by the IPCC (Seneviratne et al. 2012). CHDE occurrence is defined as when T_{\max} exceeds the 75th/90th percentile and pr is \leq the 25th/10th percentile during the study duration. Moderate CHDE is identified when T_{\max} (pr) is greater (less) than the 75th (25th) percentile, while severe CHDE occurs when T_{\max} (pr) is greater (less) than the 90th (10th) percentile.

Grid cells are labeled with "1" to indicate the occurrence of CHDE at that grid cell for the historical (1995 – 2014) and two future periods (MF: 2041 – 2060 and FF: 2081 – 2100) under the two SSPs. If a month's pr (T_{\max}) is less (greater) than the 25th (75th) percentile, then a label of 1 is given. The frequency of moderate CHDE for a year is computed by totaling the binary variables during the 12 months of that year. The same operation is performed for severe CHDE but by considering the 10th and 90th percentile for pr and T_{\max} , respectively.

The relative % change (RC) in the occurrence of CHDE events during the different periods is computed using Eq. (1)

$$RC = \frac{CF_2 - CF_1}{CF_1} \times 100\% \quad (1)$$

where CF_1 denotes compound events frequency in the historical period, while CF_2 represents CHDE events for both MF and FF periods. Previous studies have used similar

approaches (Beniston 2009; Hao et al. 2018; Zhao et al. 2023). Furthermore, trends in observed and future CHDEs are assessed based on the modified Mann–Kendall test (Eqn. S1–S4; Hamed and Rao 1998).

2.3.2 Ensemble calculation based on rank-based weighting approach

To calculate the model weights and ranking criteria, two statistical metrics, the Kling-Gupta Efficiency (KGE; Gupta et al. 2009) and the interannual variability score (IVS; Glecker et al. 2008), are used. KGE combines correlation, bias, and variability, while IVS estimates the model variability from their interannual standard deviation. Bias is computed as the ratio of modeled (μ_{cmip6}) and observed (μ_{cru}) mean values. Variability is given as the ratio of the standard deviation (STD) of the model (STD_{cmip6}) to that of observations (STD_{cru}).

The formula for computing KGE is defined in Eq. 2.

$$KGE = 1 - \sqrt{(C - 1)^2 + \left(\frac{STD_{cmip6}}{STD_{cru}} - 1\right)^2 + \left(\frac{\mu_{cmip6}}{\mu_{cru}} - 1\right)^2} \quad (2)$$

where C represents the Pearson correlation coefficient. KGE values close to 1 represent better model performance.

IVS is defined in Eq. 3.

$$IVS(cmip6, cru) = \left(\frac{STD_{cmip6}}{STD_{cru}} - \frac{STD_{cru}}{STD_{cmip6}}\right)^2, \quad (3)$$

IVS is computed using pixel-wise annual data averaged over the region. Smaller IVS values denote better model performance. Fig. S4 and Table S2 show the performance metrics of each model.

Consequently, the weights for individual GCMs are derived following their rankings from Eqs. 2 and 3. The weight of each model is derived as a function of its ranking position as defined by Eqs. 4 and 5, respectively. The equations are as follows:

$$R_i = \frac{\sum_{i=1}^N S_i}{S_i} \quad (4)$$

and

$$W_i = \frac{R_i}{\sum_{i=1}^N R_i} \quad (5)$$

where R_i is the combined performance indicator for the individual model i (higher scores indicates better model performance), S_i is the rank of each model, and N denotes the number of models. The model weight, W_i (Eq. 5) is the normalized value of R_i .

To quantify the robustness of the model multi-model ensemble (MME) computed from the rank-based weighting methods, the study employs the signal-to-noise ratio (SNR; Li et al. 2016). This approach objectively evaluates the models by considering the model spread as noise and the MME value as the signal. The change is considered robust if

models (noise) show a statistically significant change, at the same time, agree on its MME (sign). Standard deviation is used as a function to measure the model spread (Eq. 6).

$$SNR_{weighted} = \frac{\sum_i w_i \Delta p_i}{\sqrt{\sum_i w_i (\Delta p_i - \sum_i w_i \Delta p_i)^2}} \text{ for } 1 \leq i \leq 21 \tag{6}$$

Here, Δp_i signifies the i^{th} performance of each GCM, and w_i represents the weight. $SNR > 1$ indicates a robust projected change of the MME. Existing related studies across the globe have also applied the same technique (e.g., Chen et al. 2011; Li et al. 2016; Zhu et al. 2022). After the models are weighted and CHDE computed, the MME is calculated following the Eq. 7.

$$MME = W_{(mme)} = \sum (W_{(i)} \times CHDE_{(i)}) \text{ for } 1 \leq i \leq 21 \tag{7}$$

where $CHDE_{(i)}$ is the value of the i^{th} model and $W_{(i)}$ means the weight of the i^{th} model.

2.3.3 Population exposure to CHDE events

Population exposure (PE) is defined as the product of the number of people exposed to CHDEs per grid from the frequency of occurrences (Jones et al. 2015; Zhang et al. 2022; Zhao et al. 2023). In order to minimize the inter-annual variation, we adopt a 20-year average of CHDEs and population for the historical and two future periods under SSP2-4.5 and SSP5-8.5 (Liu et al. 2017; Zhang et al. 2022; Zhao et al. 2023). PE is computed using Eq. (8).

$$PE = \sum_{i=1}^{20} CHDEs_i \times P / 20 \tag{8}$$

where PE denotes the 20-year mean PE, while i signifies the i^{th} year of the historical period. $CHDEs_i$ is the value of CHDE (months) and P represents the population in units of person per day (person-day).

Furthermore, this study examines attribution factors affecting PE as proposed by Jones et al. (2015) and employed in numerous studies globally (e.g., Iyakaremye et al. 2021; Ayugi et al. 2022; Ullah et al. 2022a, b, c). The changes in exposure (ΔE) due to either human population or climatic effects or their non-linear interactions are estimated as expressed in Eq. (9).

$$\Delta E = (C_{Xh} \times \Delta P) + (P_h \times \Delta C_X) + (\Delta P \times \Delta C_X) \tag{9}$$

where C_X denotes the CHDEs, ΔP and P_h shows the incidences of CHDEs and population during the historical period, respectively, and ΔC_X shows the variations during the projected periods. $(C_{Xh} \times \Delta P)$ is an indicator of the human population effect, $(P_h \times \Delta C_X)$ estimates the climate contribution, and $(\Delta P \times \Delta C_X)$ refers to the non-linear interaction between population variation and CHDE. Ultimately, the study computes comparative contributions of each term based on Eqs. 10–12 as follows.

$$CC_{pop} = \frac{C_{Xh} \times \Delta P}{\Delta E} \times 100\% \tag{10}$$

$$CC_{clim} = \frac{P_h \times \Delta C_X}{\Delta E} \times 100\% \tag{11}$$

$$CC_{lin} = \frac{\nabla PX \nabla C_x}{\Delta E} \times 100\% \quad (11)$$

where CC_{pop} , CC_{clim} , and CC_{lin} denote the comparative contribution of change in population, climate change, and interaction factors on exposure. Recent studies applied this technique across different regions (e.g., Zhang et al. 2022; Ullah et al. 2023).

3 Results and discussions

3.1 Historical changes

Figure 1 presents the interannual variability in CHDE during the past 20 years (1995 – 2014) over EA based on CRU observations. The results show noticeable differences in moderate and severe CHDE events, with higher values in moderate CHDE. The medium value for CHDE event frequency is 1 month/year for moderate events and about 0.2 month/year for severe ones. The years 1998, 2001, 2005, and 2009 record the highest values for observed moderate CHDE events over the region, while the region experienced severe events during 2009 and 2011. Remarkably, 1995 recorded the least severe CHDE event while recording a high frequency for moderate events. A striking observation is recorded in 2005 for moderate and severe CHDE events where large variability is depicted.

These correspond to the years when the region experienced the co-occurrence of La-Nina and the negative Indian Ocean Dipole that caused suppressed precipitation and increasing temperature changes (Kebacho 2022). Conversely, 2006 recorded the lowest occurrence for both moderate and severe CHDE over the study domain. A previous study by Parhi et al. (2016) attributed the variability in weather and climate extremes to an intensification of unstable atmosphere and pronounced moisture over the region due to high SST anomalies. Moreover, the jet stream and low-level winds regulating moisture levels across EA are responsible for the positive phase of IOD regulation linked to the Indian Ocean SST anomaly (Kebacho 2022). Consequently, the changes in CHDE events could be attributed to large-scale teleconnection factors regulating climate over EA. Overall, the region

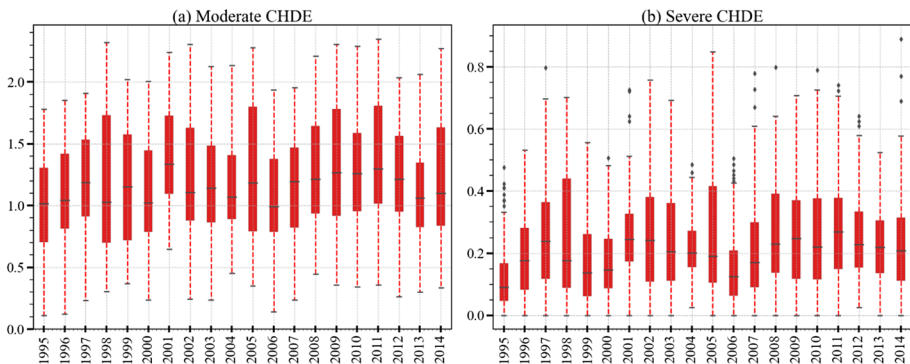


Fig. 1 Box plots of annual number of (a) moderate and (b) severe CHDE events over East Africa from observations during 1995 – 2014

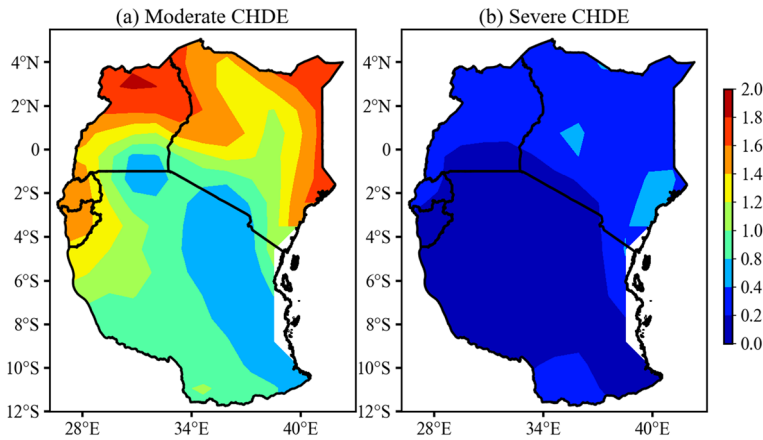


Fig. 2 Spatial distribution of (a) moderate and (b) severe CHDE events over East Africa from observations during 1995 – 2014

witnessed CHDE events, which aligns with other regions that experienced the temporal compounding of bivariate events.

For spatial changes during 1995 – 2014, it can be noted that areas around northern Uganda and northeastern Kenya are mainly affected by moderate CHDE (Fig. 2). These regions are associated with arid and semi-arid climates, which are characterized by strong winds, high temperatures, enhanced evapotranspiration rate, and low vegetation cover. In contrast, regions around Lake Victoria and parts of Tanzania record the fewest moderate and severe extreme events. For severe CHDE events, the region has experienced a homogeneous occurrence of CHDE events except for a few patches in central and coastal Kenya, where a higher frequency is noted (Fig. 2b). The historical changes show that a large section of Tanzania experienced less severe CHDE during the study period.

The current study agrees with other recent studies that have demonstrated an increase in CHDE events, which corresponds to the manifestation of heatwaves and droughts across many regions of the world (Zscheischler and Seneviratne 2017; Meng et al. 2022; Wu et al. 2021). In fact, a robust increase in these compound events has been reported to be more prominent in Africa, China and Australia (Wu et al. 2021). Compared to the 1950s, when unequivocal global warming was first reported in the fifth IPCC assessment report, the number of hot-dry and hot-wet events has intensified tenfold over many regions of the world during the last 20 years (IPCC et al. 2021). Quantifying the observed changes over EA, which remains susceptible to climate change, contributes to hazard risk management and helps accurately estimate projected changes.

3.2 Model evaluation and weighting

Before employing GCMs to estimate the future changes in CHDEs over the EA region, all models are evaluated to identify the best-performing ones. This study uses KGE and inter-annual variability score (IVS) to examine how observed T_{max} and precipitation skillfully replicate the observed climatology. Fig. S4 and Table S2 summarize the model performance over the study region. Overall, most CMIP6 models show good skills in simulating

Table 1 Weights and ranks of the 21 GCMs based on their performance in East Africa. Bolded values indicate models with a weight > 0.048 (0.048 is the value of equally weighted models). Models are ranked according to the statistical metrics as presented in Eqs. 2, 3, 4, and 6

Models	C	β	IVS	KGE	Sum of the ranks	Weights
UKESM1-0-LL	5	2	5	1	13	0.134
FGOALS-g3	12	1	6	2	21	0.083
MPI-ESM1-2-HR	13	4	1	4	22	0.079
ACCESS-CM2	15	3	2	6	26	0.067
MPI-ESM1-2-LR	10	11	3	5	29	0.060
INM-CM5-0	2	17	7	8	34	0.051
NESM3	3	13	13	7	36	0.049
GFDL-CM4	4	14	16	3	37	0.047
CanESM5	1	10	21	10	42	0.042
BCC-CSM2-MR	11	8	9	18	46	0.038
MRI-ESM2-0	9	5	19	13	46	0.038
MIROC-ES2L	6	18	14	9	47	0.037
IPSL-CM6A-LR	7	20	11	11	49	0.036
ACCESS-ESM1-5	18	7	12	14	51	0.034
INM-CM4-8	8	21	10	12	51	0.034
EC-Earth3	19	6	15	15	55	0.032
CNRM-ESM2	20	12	4	20	56	0.031
EC-Earth3-Veg	17	9	17	17	60	0.029
CNRM-CM6	21	16	8	21	66	0.026
GFDL-ESM4	16	15	18	19	68	0.026
MIROC6	14	19	20	16	69	0.025

C: correlation coefficient; β : Bias

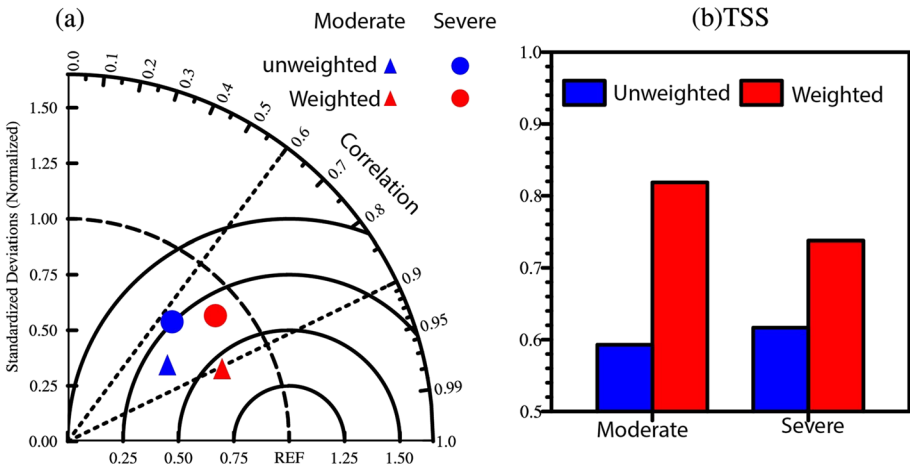


Fig. 3 (a) Taylor Diagram and (b) Taylor Skill Score (TSS) for weighted and unweighted multi-model ensembles for moderate and severe CHDE events during 1995 – 2014

monthly precipitation and T_{max} with a $KGE > 0.6$ and a small IVS , especially for T_{max} . The results of these metrics (KGE and IVS) are subsequently used to derive the weights for the GCMs. The weights for the models used are shown in Table 1, following the approach described in Section 2.3.2.

The resulting MMEs computed using the weighted technique (Chen et al. 2011) and normal arithmetic computation (unweighted) are shown in Fig. 3 and Table 1. Comparing the two MMEs based on the Taylor diagram and Taylor Skill Score (TSS; Taylor 2001) shows that the weighted MME performs better than the unweighted MME. The unweighted (weighted) MME shows a spatial correlation coefficient of 0.6 (0.8 and 0.9 for moderate and severe CHDE events, respectively). The clear evidence of improved performance is noted in TSS, where the unweighted MME shows TSS values of 0.58 and 0.6 for moderate and severe CHDE, whereas the weighted MME depicts TSS values of 0.82 and 0.76, respectively. The results demonstrate the need to employ a weighting approach to optimize MME performance.

The capability of weighted MME is further evaluated in terms of its ability to capture spatial changes. Figure 4 shows the spatial variance of weighted and unweighted MME in simulating moderate and severe CHDEs during 1995–2014 over EA. Unweighted (weighted) MME minus OBS shows a bias of 0.40 (0.24) and 0.12 (0.07) for moderate and severe CHDEs, respectively (Fig. 4). Overall, the results demonstrate that model weighting can help to minimize the total uncertainty of climate model projection (Brunner et al. 2019). Numerous approaches have been employed in the past with the premise that a model’s capability to accurately reproduce historical climate can be used to predict

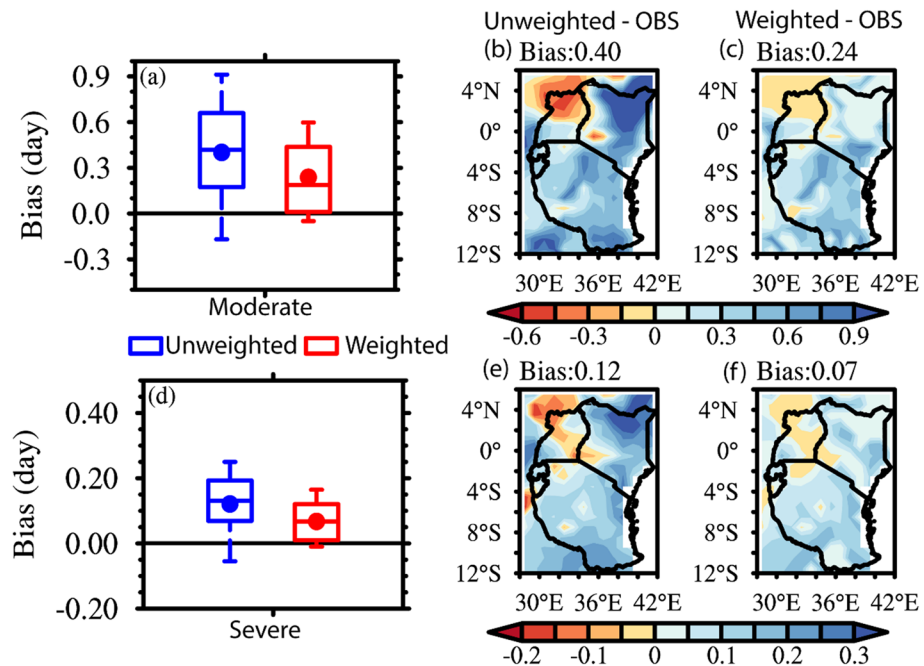


Fig. 4 Spatial plot of bias for weighted and unweighted multi-model ensembles. (a, b, c) moderate and (d, e, f) severe CHDE events

a model's future dependability. The models that perform better are given more weights when computing the MME. Thus, the current study calculates MME based on the weighted approach for the projection of CHDEs during MF and FF. A similar approach has been employed over different regions to attain reliable estimates of future climate (Knutti et al. 2017; Li et al. 2021; Zhu et al. 2023).

3.3 Projected changes

Figure 5 presents the results for projected changes in the mean annual frequency of CHDE events over EA under SSP2-4.5 and SSP5-8.5 relative to baseline period of 1995–2014. Moderate CHDEs will occur twice more frequently, while the frequency of severe CHDE will be 1.6 times that of baseline (i.e., an increase of 60%) under the SSP5-8.5 scenario. Strong evidence of an upward trajectory is noted after 2080 for both moderate and severe CHDE. Under SSP2-4.5, moderate and severe CHDEs are estimated to decrease after 2090 as global greenhouse gas emissions are anticipated to reach zero levels under manageable practices. However, a sustained increase in CHDE is projected under SSP5-8.5, which represents the Anthropocene pathways characterized by strong radiative forcing (O'Neill et al. 2017). Overall, these expected changes in CHDE events are likely to be more pronounced in the future, calling for relevant policy designs that would lessen the effects of associated disaster risks.

Figure 6 shows the spatial changes in CHDE events under the SSP2-4.5 and SSP5-8.5 scenarios during the MF and FF relative to the historical period. The dots represent regions where SNR is greater than 1. This implies robust future projection due to the clear signal compared to noise (Hawkins and Sutton 2011; Dosio et al. 2019; IPCC et al. 2021). It is apparent that greatest impact of CHDE of upto about 140% increase will be experienced during FF period in all the two scenarios as compared to MF. Strong evidence of moderate CHDE events is projected to occur under SSP2-4.5 during MF as compared to high emission scenario during similar time period (Fig. 6 a, e). On the other hand, no remarkable increase in projected to occur for severe CHDE events under SSP5-8.5, with the region depicting homogenous spatial variance of the event (Fig. 6f). Interestingly, southern parts of Tanzania will experience an exacerbated increment of moderate and severe CHDE events of upto 140% during FF period (Fig. 6d, h). The robustness of the change

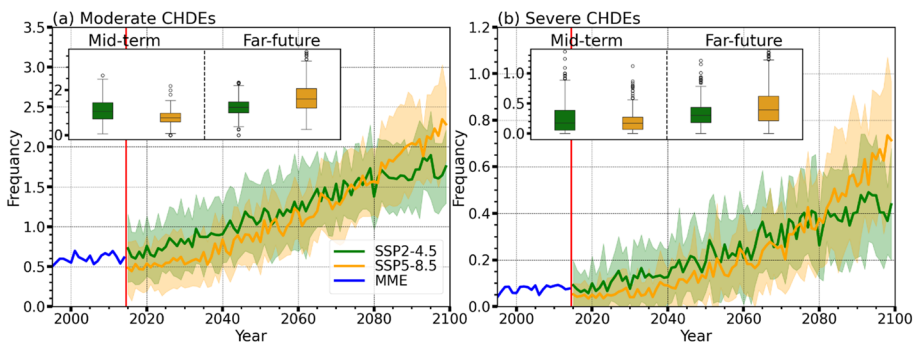


Fig. 5 Projected interannual variability of (a) moderate and (b) severe CHDE events under SSP2-4.5 (green) and SSP5-8.5 (orange) relative to baseline period of 1995 – 2014 (blue). The shading denotes the uncertainty range (± 1 standard deviation of the model annual average). The insets indicate the multi-year average frequency for the mid-future (2041–2060) and far-future (2081–2100) periods

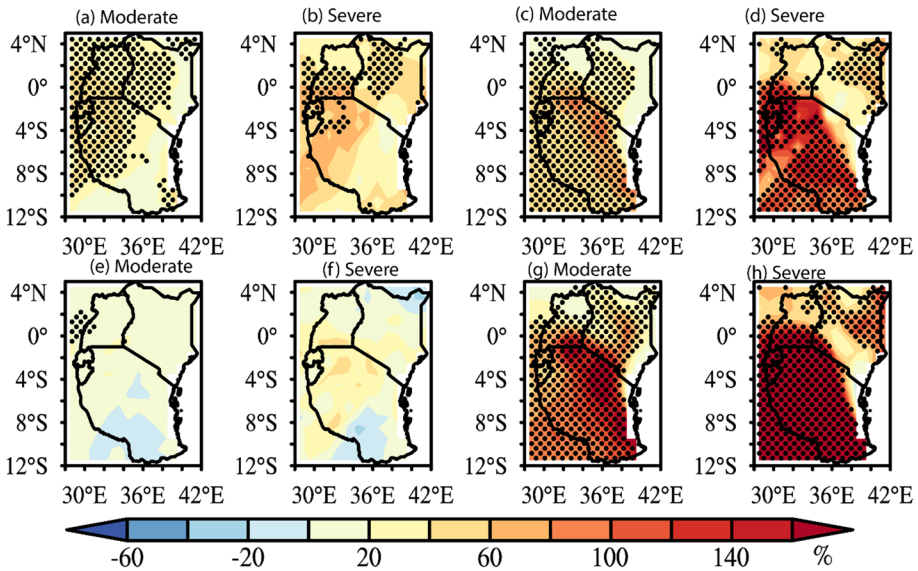


Fig. 6 Spatial variation in the change in frequency (units: %) of CHDE events under (a–d) SSP2-4.5 and (e–h) SSP5-8.5 relative to the historical period (1995 – 2014). (a, e) moderate CHDE during MF (2041–2060), (b, f) severe CHDE during MF (c, g) moderate CHDE during FF (2081–2100), and (d, h) severe CHDE during FF. The dots represent grids where $SNR > 1$

is demonstrated with model agreement depicting $SNR > 1$ for both scenarios during FF period. Comparing the two results of different scenario, the projected change under SSP5-8.5 during the MF shows lower occurrences of moderate and severe CHDE, especially over Kenya, Uganda, Burundi, and Rwanda (Fig. 6e, f). In contrast, largest increase in CHDE for moderate and severe events is noted in SSP2-4.5 as compared to SSP5-8.5 scenario (Fig. 6a, b). Interestingly, there is no significant difference in severe CHDE events during FF for both scenarios. The reduced impact of CHDE events under SSP5-8.5 scenario during MF period compared to SSP2-4.5 could be attributed to the pronounced wetting during the same period as projected in recent existing studies (Tierney et al. 2015; Ongoma et al. 2018; Scoccimarro and Gualdi 2020; Ayugi et al. 2021b, 2023). These studies reported a ‘recovery pattern’ of rainfall event over the region since 1999 when an abrupt decline in long rains was reported, thus plunging the region to recurrent drought events (Lyon and DeWitt 2012). However, recent study by Palmer et al. (2023) noted that climate models project that the region will experience more rainfall during 2030 – 2040, with implication of sustaining agricultural yields and thus offsetting high air temperature (i.e., hot extremes) and low atmospheric humidity (i.e., dry extremes). Thus, low values of CHDE occur during MF under high emission scenario relative to the baseline period. These results provide an important insight into CHDE events that could lead to more heatwave and drought events, especially during the FF periods under different scenarios. Tanzania and northeast Kenya are likely to be most affected, with all models agreeing ($SNR > 1$) on a likely higher magnitude of change during both MF and FF periods.

Meanwhile, the results of the current study agree with previous studies that have also noted a higher magnitude of change in CHDE events across different regions (Weber et al. 2020; Ullah et al. 2022a, b; Meng et al. 2022; Dosio et al. 2023). For illustration, the previous study that analyzed compound climate extremes over Africa and employed regional

climate models sourced from CODEX-CORE revealed an increase in the frequency of events, with pronounced changes larger in the business-as-usual scenario as compared to that of the moderate scenario (Weber et al. 2020). The study further reported that West Africa, Central Africa, Mediterranean, and Eastern Southern Africa would be predominantly affected. Over EA, Muheki et al. (2024) highlighted that compound events such as wildfires and heatwaves will rise by the largest magnitude (+940%) by 2100, followed by river floods and wildfires (+250%) under RCP6.0 scenarios. This study also pointed out that concurrent CHDE events will be the norm rather than an exception in the study region, even under “very stringent” pathways, which is also reflected in the current study. Over Europe, Dosio et al. (2023) observed that even under SSP1-2.6 pathways, climate models predict an intensification of CHDE events across large areas (>60%) of Europe. Meanwhile, Zhang et al. (2021) noted that compound extremes are mainly influenced by semi-permanent circulations, strong high-pressure systems, and Rossby wave patterns, mainly modulated by atmosphere-land feedback. Overall, regions such as EA, which have weak governance systems, are likely to be most affected compared to nations with strong institutional systems (Tabari and Willems 2023). Thus, these results underscore the need to quantify PE and the main attributing factors that drive the projected changes in CHDE events over the study domain.

3.4 Population exposure changes and attribution factors

With clear evidence that CHDE events are projected to intensify in the EA region, it is necessary to estimate the affected population in order to design mitigation strategies to curb the effects of climate change. Figure 7 shows the relative change in exposure across



Fig. 7 Relative changes (unit: %) in the multi-year average population exposure under (a–d) SSP2-4.5/SSP2, and (e–h) SSP5-8.5/SSP5 compared to the historical period (1995 – 2014). (a, e) moderate CHDE during MF (2041–2060), (b, f) severe CHDE during MF (2081–2100), (c, g) moderate CHDE during FF (2081–2100), and (d, h) severe CHDE during FF. Hatched areas indicate regions that are significant at a 95% significant level

the EA region during future timescales, considering the two emission scenarios. The significant exposure is more prominent in regions of Mbeya and Iringa in southern Tanzania and Marsabit, Isiolo, and Samburu counties in Kenya for moderate and severe extremes. For instance, under the SSP2-4.5 scenario, average PE in the MF and FF shows that moderate CHDE events will be most prominent in southern parts of Tanzania while severe CHDE events will affect northeastern parts of Kenya (Fig. 7a and b). Further analysis shows that the relative change in PE to moderate and severe CHDE will be less under the SSP5-8.5 scenario during MF, especially in regions along Rwanda, Burundi, and parts of Mount Elgon between Kenya and Uganda border (Fig. 7e and f). However, PE is projected to increase by 20% during the FF period for most regions, except for southern Tanzania, which will experience up to 40–60% change (Figs. 7g and 7h). No significant change in PE is projected to occur in regions of Kenya, Uganda, Burundi, and Rwanda for severe CHDE events during FF under SSP5-8.5 (Fig. 7g and h). However, PE is projected to increase significantly along parts of southern Tanzania by up to 60% for moderate and severe CHDEs. Interestingly, only southern Tanzania is projected to experience significant PE change for moderate CHDE under SSP2-4.5 during the FF period (Fig. 7c). These results suggest that regions that will be mainly affected in compound extremes should consider implementing appropriate adaptation strategies to cope with the impending exposure to moderate and severe CHDEs.

It is interesting to note that a previous study that estimated future changes in PE to extremely wet days (R95p) showed that Uganda, Burundi, and Rwanda will experience the most prominent and net intense effects (Ayugi et al. 2022). In contrast, the study revealed that minimal change is projected to occur in Kenya and Tanzania. This shows a dipole scenario in regions affected by two different extreme climate events, R95p and CHDE. Similarly, a study that explored the projected change in maximum daily maximum temperature (TXx) and the associated population revealed that some regions in EA cities would be affected by up to about 12 million people exposed (Iyakaremye et al. 2021). The study reported that PE will increase by 25%–45% from the base period under varying scenarios. In agreement with a similar study conducted over the African continent (Weber et al. 2020), the study reported that coincident heatwaves will mostly affect West and Central equatorial Africa, Southeast Africa and East Madagascar. Meanwhile, in China, Zhao et al. (2023) noted that PE to moderate and severe CHDE events will increase from 0 to 10% and 30 to 50%, respectively. The study further noted that CHDE events in northeast China and some parts of Suchuan city would decline, while western and southern China would experience a significant increase in CHDE PE. At the global level, Liu et al. (2017) reported that exposure will be the highest in Nigeria, Central America and Indonesia. The study concluded that Africa will experience the largest effect, nearly 120 times its current value. Such changes call for urgent adaptation and mitigation actions to cushion the population from the effects of climate change.

To further quantify the number of persons exposed to CHDE events during the MF and FF periods, this study quantifies the number of populations exposed to CHDE severity. Figure 8 shows the regional aggregate annual exposure for historical periods, MF and FF, to moderate and severe CHDE events. During the historical period, the exposure is 15 billion person-day on average for moderate CHDE exposure and 14 billion person-day for severe CHDE (Figs. 8a and b). In contrast, during the MF period, the estimated exposure is projected to increase to 65 billion person-day for the moderate extreme under SSP2-4.5|SSP2 scenario and 43 billion person-day under SSP5-8.5|SSP5. Remarkably, the largest change is noted during the FF period, where exposure to moderate extremes will persist to increase to ~ 120 (100) billion person-day under SSP2-4.5|SSP2 (SSP5-8.5|SSP5) (Fig. 8a). Notably,

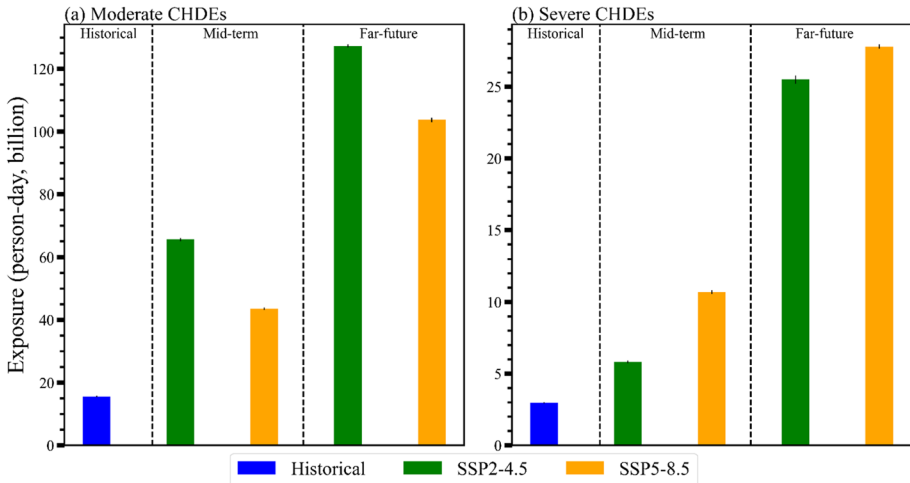


Fig. 8 Multi-year average population exposure (units: billion persons-day) to (a) moderate and (b) severe CHDE events for the historical (blue bars) and projection periods (mid-future: 2041–2060 and far-future: 2081–2100)

the PE to severe CHDE events is projected to be less as compared to moderate events during MF period. Specifically, the area cumulative annual exposure for SSP2-4.5/SSP2 scenario is about 8 billion person-day while at 11 billion person-day for SSP5-8.5/SSP5 scenario. However, the largest exposure is projected to occur in severe CHDEs compared to moderate events under the SSP5-8.5/SSP5 scenario. For instance, the PE to severe CHDE will outweigh the moderate events by about a 12 billion person-day difference. This calls for exploring attribution factors responsible for the increase in exposure to severe CHDE during the FF period under the high-emission scenario.

Consequently, the study explores the relative contribution of different influences such as population, climate change, and non-linear effects of population and climate as defined in Eq. (9). This concurs with other existing studies across different locales (Liu et al. 2017; Ayugi et al. 2021a; Zhao et al. 2023; Sun et al. 2023; Zhang et al. 2022). Figure 9 shows the PE to CHDE attribution drivers for SSP2-4.5/SSP2 and SSP5-8.5/SSP5 scenarios. The findings demonstrate that the climate effect is the main driving factor for exposure to CHDE under the two emission pathways. In fact, the findings show a pronounced contribution of climate factor under SSP5-8.5/SSP5 with PE totaling 25×10^5 billion person-day. Under the two pathways considered, climate factors and population effects demonstrate a greater contribution to PE-CHDE events. However, comparing the climate effect under SSP2-4.5/SSP2 and SSP5-8.5/SSP5, the results show a lower contribution of climate effect under the moderate pathway scenario. The human-induced climate change not only has an impact on CHDE but also significantly contributes to the rapid intensification of other extreme events, such as flash droughts (Christian et al. 2021; Wang et al. 2021; Ullah et al. 2024) and heatwaves (Ma et al. 2023). Interestingly, the contribution of population growth to an increase in exposure depicts a much lower contribution to CHDE exposure, unlike the previous study that reported the contribution of population effect to net exposure to very wet extreme events (Ayugi et al. 2022). This shows that CHDE is mainly driven by

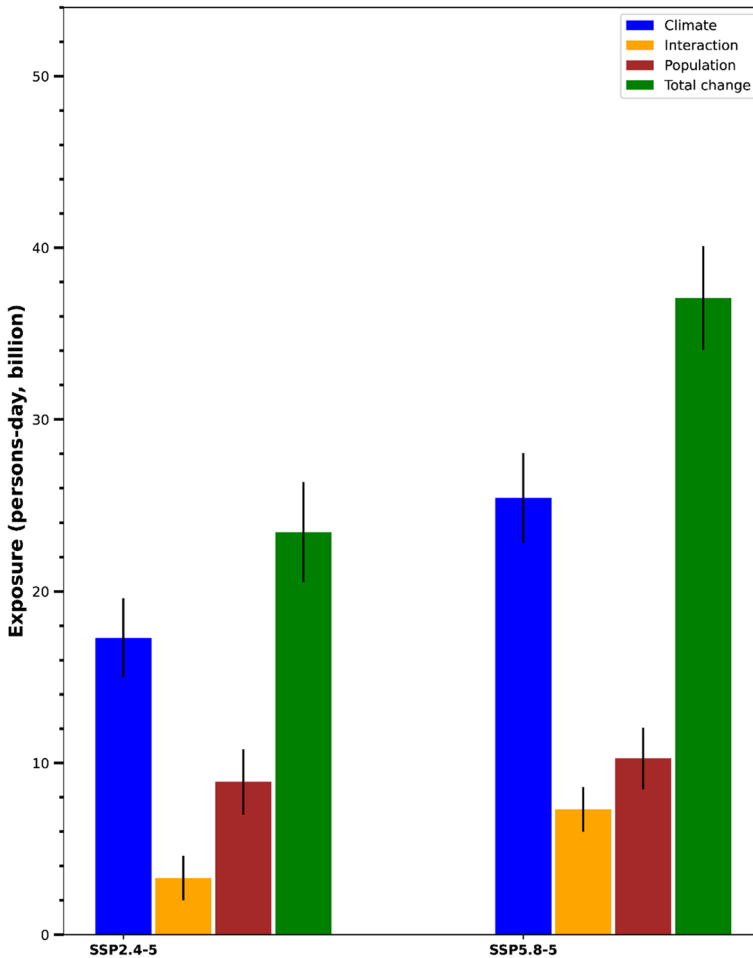


Fig. 9 Relative contribution analysis of influencing factors under SSP2-4.5|SSP2 and SSP5-8.5|SSP5. Blue, orange, brown and green bars represent climate effects, interaction effects, population effects and total change effects on projected changes in exposure to CHDE events, respectively. The error bars show the standard deviation in total projected change across the models for East Africa

an increase in temperature, which is projected to continue increasing under all scenarios (IPCC 2021). In fact, it is reported that over Africa, TX_x is likely to exceed 1.82 °C and 3 °C under SSP2-4.5 and SSP5-8.5, respectively (Iyakaremye et al. 2021). Almazroui et al. (2021) further noted that hot temperature extremes will experience an increase in intensity and frequency over specific hotspot regions. Overall, the current study calls for the need to reduce CO₂ emission, which remains the main driving force behind the increase in temperature, thereby enhancing the climate effect as the main attributing factor to the effect of CHDE events over EA and other regions, as reported in the existing studies.

4 Conclusion

This study's findings indicate that the East African region experienced numerous moderate and severe CHDE events during the past twenty years. Based on a weighted MME, projections show that the frequency of moderate CHDEs will double, while severe CHDE will increase by 60% relative to the historical period under the SSP5-8.5 scenario. Southern parts of Tanzania and northeastern Kenya are likely to be most affected, with all models agreeing (SNR > 1) on a likely higher magnitude of change during both the MF and FF periods. The resultant impact on the population is significant, with exposure projected to increase significantly along parts of southern Tanzania by up to 60% for moderate and severe CHDE. Attribution factors highlight that climate change is the main driving factor behind increased exposure to CHDEs under the two emission pathways.

The present study underscores the need to reduce CO₂ emissions, which remain the main driver of the increase in temperature and, consequently, the increased occurrence of CHDE events over EA and other regions, as reported in the existing studies. The findings highlight the need to further explore multi-variate analyses by examining more than two extreme events occurring simultaneously in the same locality. A recent study (Muheki et al. 2024) over EA reported an increase in co-occurring extremes such as; (i) river floods and wildfire, (ii) river floods and heatwaves and (iii) heatwaves and wildfires, thus, there is a need for multi-variate analysis of such extreme events. Moreover, additional research is recommended to investigate underlying mechanisms and their influence on compound events across the region. Despite the robust findings, some unavoidable uncertainties in the projection of CHDE events should be noted. These uncertainties can arise from climate models or climate scenarios (Brunner et al. 2019). Therefore, it is suggested that more models and emission scenarios from the CMIP6 family be included in future studies to enhance the accuracy of climate projections of compound extremes.

Supplementary Information The online version contains supplementary material available at <https://doi.org/10.1007/s10584-024-03802-6>.

Acknowledgements The authors acknowledge the producers of the observation, model and population datasets for making their products openly available.

Authors contribution All authors have made equal contributions during the manuscript preparation.

Funding This research was supported by the Brain Pool program funded by the Ministry of Science and ICT through the National Research Foundation of Korea (Grant number: 2022H1D3A2A02063155).

Data availability CMIP6: <https://esgf-node.llnl.gov/projects/esgf-llnl/>

Gridded Population of the World (GPWv3): <http://sedac.ciesin.columbia.edu/data/collection/gpw-v3>

CRU: https://crudata.uea.ac.uk/cru/data/hrg/cru_ts_4.05/cruts.2103051243.v4.05/

Declarations

Declaration of generative AI in scientific writing The authors declare that no part of the draft applied AI or AI-assisted technology in the writing process.

Competing interests The authors have no relevant financial or non-financial interests to disclose.

References

- Akinsanola AA, Ongoma V, Kooperman GJ (2021) Evaluation of CMIP6 models in simulating the statistics of extreme precipitation over Eastern Africa. *Atmos Res* 254:105509. <https://doi.org/10.1016/j.atmosres.2021.105509>
- Almazroui M, Saeed F, Saeed S, Nazrul Islam M, Ismail M, Klutse NAB, Siddiqui MH (2020a) Projected change in temperature and precipitation over Africa from CMIP6. *Earth Syst Environ* 4:455–475. <https://doi.org/10.1007/s41748-020-00161-x>
- Almazroui M, Saeed F, Saeed S, Ismail M, Ehsan MA, Islam MN ... Nadeem I (2021) Projected changes in climate extremes using CMIP6 simulations over SREX regions. *Earth Syst Environ* 5(3):481–497. <https://doi.org/10.1007/s41748-021-00250-5>
- Aghakouchak A, Chiang F, Huning LS, Love CA, Mallakpour I, Mazdiyasi O et al (2020) Climate extremes and compound hazards in a warming world. *Annu Rev Earth Pl SC* 48:519–548. <https://doi.org/10.1146/annurev-earth-071719-055228>
- Almazroui M, Saeed S, Saeed F, Islam MN, Ismail M (2020b) Projections of precipitation and temperature over the South Asian countries in CMIP6. *Earth Syst Environ* 4:297–320. <https://doi.org/10.1007/s41748-020-00157-7>
- Ayugi BO, Wen W, Chepkemoi D (2016) Analysis of spatial and temporal patterns of rainfall variations over Kenya. *J Environ Earth Sci* 6(11):69–83
- Ayugi B, Jiang Z, Zhu H, Ngoma H, Babausmail H, Rizwan K, Dike V (2021a) Comparison of CMIP6 and CMIP5 models in simulating mean and extreme precipitation over East Africa. *Int J Climatol* 41(15):6474–6496. <https://doi.org/10.1002/joc.7207>
- Ayugi B, Dike V, Ngoma H, Babausmail H, Mumo R, Ongoma V (2021b) Future changes in precipitation extremes over East Africa based on CMIP6 models. *Water* 13(17):2358. <https://doi.org/10.3390/w13172358>
- Ayugi B, Jiang Z, Iyakaremye V, Ngoma H, Babausmail H, Onyutha C, Dike VN, Mumo R, Ongoma V (2022) East African population exposure to precipitation extremes under 1.5 °C and 2.0 °C warming levels based on CMIP6 models. *Environ Res Lett* 17(4). <https://doi.org/10.1088/1748-9326/ac5d9d>
- Ayugi BO, Chung ES, Zhu H, Ogega OM, Babousmail H, Ongoma V (2023) Projected changes in extreme climate events over Africa under 1.5°C, 2.0 C and 3.0°C global warming levels based on CMIP6 projections. *Atmos Res* 106872. <https://doi.org/10.1016/j.atmosres.2023.106872>
- Beniston M (2009) Trends in joint quantiles of temperature and precipitation in Europe since 1901 and projected for 2100. *Geophys Res Lett* 36:6. <https://doi.org/10.1029/2008gl037119>
- Bevacqua E, Suarez-Gutierrez L, Jézéquel A, Lehner F, Vrac M, Yiou P, Zscheischler J (2023) Advancing research on compound weather and climate events via large ensemble model simulations. *Nat Commun* 14(1):2145. <https://doi.org/10.1038/s41467-023-37847-5>
- Brunner L, Lorenz R, Zumwald M, Knutti R (2019) Quantifying uncertainty in European climate projections using combined performance-independence weighting. *Environ Res Lett* 14(12):124010. <https://doi.org/10.1088/1748-9326/ab492f>
- Camara M, Diba I, Diedhiou A (2022) Effects of land cover changes on compound extremes over West Africa using the regional climate model regCM4. *Atmosphere* 13(3):421. <https://doi.org/10.3390/atmos13030421>
- Chen W, Jiang Z, Li L (2011) Probabilistic projections of climate change over China under the SRES A1B scenario using 28 AOGCMs. *J Clim* 24(17):4741–4756. <https://doi.org/10.1175/2011JCLI4102.1>
- Christian JI, Basara JB, Hunt ED, Otkin JA, Furtado JC, Mishra V et al (2021) Global distribution, trends, and drivers of flash drought occurrence. *Nat Commun* 12(1):6330. <https://doi.org/10.1038/s41467-021-26692-z>
- Deegala D, Song YH, Chung ES, Ayugi BO, and Shahid S (2023) Future extreme precipitation changes in the South Asian summer monsoon dominance region. *Atmos Res* 295:107029. <https://doi.org/10.1016/j.atmosres.2023.107029>
- Dioha EC, Chung ES, Ayugi BO, Babausmail H, and Lim Kam Sian KTC (2024) Quantifying the added value in the NEX-GDDP-CMIP6 models as compared to native CMIP6 in simulating Africa's diverse precipitation climatology. *Earth Syst Environ* 8(2):417–436. <https://doi.org/10.1007/s41748-024-00397-x>
- Dosio A, Jones RG, Jack C, Lennard C, Nikulin G, Hewitson B (2019) What can we know about future precipitation in Africa? Robustness, significance and added value of projections from a large ensemble of regional climate models. *Clim Dyn* 53:5833–5858. <https://doi.org/10.1007/s00382-019-04900-3>
- Dosio A, Spinoni J, Migliavacca M (2023) Record-breaking and unprecedented compound hot and dry summers in Europe under different emission scenarios. *Environ Res: Climate* 2(2023):045009. <https://doi.org/10.1088/2752-5295/acfa1b>

- Eyring V, Bony S, Meehl G, Senior C, Stevens B, Stouffer R, Taylor K (2016) Overview of the coupled model intercomparison project phase 6 (CMIP6) experimental design and organization. *Geosci Model Dev* 9(5):1937–1958. <https://doi.org/10.5194/gmd-9-1937-2016>
- Funk C, Harrison L, Segele Z, Rosenstock T, Steward P, Anderson CL ... Hughes D (2023) Tailored forecasts can predict extreme climate informing proactive interventions in East Africa. *Earth's Future* 11(7): e2023EF003524. <https://doi.org/10.1029/2023EF003524>
- Hamed KH, Ramachandra Rao A (1998) A modified Mann-Kendall trend test for autocorrelated data. *J Hydrol* 204:182–196. [https://doi.org/10.1016/S0022-1694\(97\)00125-X](https://doi.org/10.1016/S0022-1694(97)00125-X)
- Hao Z, AghaKouchak A, Phillips TJ (2013). Changes in concurrent monthly precipitation and temperature extremes. *Environ Res Lett* 8(3):034014. <https://doi.org/10.1088/1748-9326/8/3/034014>
- Hao Z, Hao F, Singh VP, Zhang X (2018) Changes in the severity of compound drought and hot extremes over global land areas. *Environ Res Lett* 13(12):124022. <https://doi.org/10.1088/1748-9326/13/12/124022>
- Hao Y, Hao Z, Feng S, Zhang X, Hao F (2020) Response of vegetation to El Niño-Southern Oscillation (ENSO) via compound dry and hot events in southern Africa. *Glob Planet Change* 195:103358. <https://doi.org/10.1016/j.gloplacha.2020.103358>
- Gleckler PJ, Taylor KE, Doutriaux C (2008) Performance metrics for climate models. *J Geophys Res* 113:D06104. <https://doi.org/10.1029/2007JD008972>
- Gupta HV, Kling H, Yilmaz KK, Martinez GF (2009) Decomposition of the mean squared error and NSE performance criteria: Implications for improving hydrological modelling. *J Hydrol* 377(1–2):80–91. <https://doi.org/10.1016/j.jhydrol.2009.08.003>
- Haile GG, Tang Q, Leng G, Jia G, Wang J, Cai D et al (2020) Long-term spatiotemporal variation of drought patterns over the Greater Horn of Africa. *Sci Total Environ* 704:135299. <https://doi.org/10.1016/j.scitotenv.2019.135299>
- Harris I, Osborn TJ, Jones P, Lister D (2020) Version 4 of the CRU TS monthly high-resolution gridded multivariate climate dataset. *Sci Data* 7:109. <https://doi.org/10.1038/s41597-020-0453-3>
- Hawkins E, Sutton R (2011) The potential to narrow uncertainty in projections of regional precipitation change. *Clim Dyn* 37:407–418. <https://doi.org/10.1007/s00382-010-0810-6>
- Iturbide M, Gutiérrez JM, Alves LM et al (2020) An update of IPCC climate reference regions for subcontinental analysis of climate model data: Definition and aggregated datasets. *Earth Syst Sci* 12:2959–2970. <https://doi.org/10.5194/essd-2019-258>
- IPCC Seneviratne SI, Zhang X, Adnan M, Badi W, Dereczynski C, Di Luca A, Ghosh S, Iskandar I, Kossin J, Lewis S, Otto F, Pinto I, Satoh M, VicenteSerrano SM, Wehner M, Zhou B (2021) Weather and climate extreme events in a changing climate. The Physical science basis. Contribution of working group I to the sixth assessment report of the intergovernmental panel on climate change. In: Masson-Delmotte V, Zhai P, Pirani A, Connors SL, Péan C, Berger S, Caud N, Chen Y, Goldfar L, Gomis MI, Huang M, Leitzell K, Lonnoy E, Matthews JBR, Maycock TK, Waterfield T, Yelekçi O, Yu R, Zhou B (eds) Cambridge University Press, Cambridge and New York, p 2391. <https://doi.org/10.1017/9781009157896>
- Iyakaremye V, Zeng G, Yang X, Zhang G, Ullah I, Gahigi A, Vuguziga F, Asfaw TG, Ayugi B (2021) Increased high-temperature extremes and associated population exposure in Africa by the mid-21st century. *Sci Total Environ* 790:148162. <https://doi.org/10.1016/j.scitotenv.2021.148162>
- Jones B, O'Neill BC, McDaniel L, McGinnis S, Mearns LO, Tabladi C (2015) Future population exposure to US heat extremes. *Nat Clim Change* 5:652–655. <https://doi.org/10.1038/nclimate2631>
- Jones B, O'Neill BC (2016) Spatially explicit global population scenarios consistent with the Shared Socio-economic Pathways. *Environ Res Lett* 11:084003. <https://doi.org/10.1088/1748-9326/11/8/084003>
- Kebacho LL (2022) Large-scale circulations associated with recent interannual variability of the short rains over East Africa. *Meteorol Atmos Phys* 134(1):10. <https://doi.org/10.1007/s00703-021-00846-6>
- Knutti R, Sedláček J, Sanderson BM, Lorenz R, Fischer EM, Eyring V (2017) A climate model projection weighting scheme accounting for performance and interdependence. *Geophys Res Lett* 44:1909–1918. <https://doi.org/10.1002/2016GL072012>
- Li W, Jiang Z, Xu J, Li L (2016) Extreme precipitation indices over China in CMIP5 models. Part II: probabilistic projection. *J Clim* 29(24):8989–9004. <https://doi.org/10.1175/JCLI-D-16-0377.1>
- Li T, Jiang Z, Zhao L, Li L (2021) Multi-model ensemble projection of precipitation changes over China under global warming of 1.5 and 2°C with consideration of model performance and independence. *J Meteor Res* 35:184–197. <https://doi.org/10.1007/s13351-021-0067-5>
- Liu Z, Anderson B, Yan K, Dong W, Liao H, Shi P (2017) Global and regional changes in exposure to extreme heat and the relative contributions of climate and population change. *Sci Rep* 7:43909. <https://doi.org/10.1038/srep43909>
- Lu K, Arshad M, Ma X, Ullah I, Wang J, Shao W (2022) Evaluating observed and future spatiotemporal changes in precipitation and temperature across China based on CMIP6-GCMs. *Int J Climatol* 42(15):7703–7729. <https://doi.org/10.1002/joc.7673>

- Lyon B, DeWitt DG (2012) A recent and abrupt decline in the East African long rains. *Geophys Res Lett* 39(2). <https://doi.org/10.1029/2011JGL050337>
- Ma F, Yuan X (2023) When will the unprecedented 2022 summer heat waves in Yangtze River Basin become normal in a warming climate? *Geophys Res Lett* 50(4):1–12. <https://doi.org/10.1029/2022GL101946>
- Meng Y, Hao Z, Feng S, Zhang X, Hao F (2022) Increase in compound dry-warm and wet-warm events under global warming in CMIP6 models. *Glob Planet Change* 210:103773. <https://doi.org/10.1016/j.gloplacha.2022.103773>
- Muheki D, Deijns AAJ, Bevacqua E, Messori G, Zscheischler J, Thiery W (2024) The perfect storm? Concurrent climate extremes in East Africa. *Egusphere* 2023:1–40. <https://doi.org/10.5194/egusphere-2023-1712>
- Niang I, Ruppel OC, Abdrabo MA, Essel A, Lennard C, Padgham J, Urquhart P (2014) Climate change 2014: impacts, adaptation, and vulnerability. Part B: Regional aspects. Contribution of working group II to the Fifth Assessment. In: Barros VR, Field CB, Dokken DJ et al (eds) Intergovernmental panel on climate change. Cambridge University Press, Cambridge and New York, pp 1199–1265. <https://doi.org/10.1017/CBO9781107415386.002>
- Nicholson SE (2017) Climate and climatic variability of rainfall over eastern Africa. *Rev Geophys* 55(3):590–635. <https://doi.org/10.1002/2016RG000544>
- Nooni IK, Ogou FK, Chaibou AAS, Nakoty FM, Gnitou GT, Lu J (2023) Evaluating CMIP6 historical mean precipitation over Africa and the Arabian Peninsula against satellite-based observation. *Atmosphere* 14(3):607. <https://doi.org/10.3390/atmos14030607>
- Obahoundje S, Nguessan-Bi VH, Diedhiou A, Kravitz B, Moore JC (2023) Implication of stratospheric aerosol geoengineering on compound precipitation and temperature extremes in Africa. *Sci Total Environ* 863:160806. <https://doi.org/10.1016/j.scitotenv.2022.160806>
- Omondi OA, Lin Z (2023) Trend and spatial-temporal variation of drought characteristics over equatorial East Africa during the last 120 years. *Front Earth Sci* 10:1064940. <https://doi.org/10.3389/feart.2022.1064940>
- Ongoma V, Chen H (2017) Temporal and spatial variability of temperature and precipitation over East Africa from 1951 to 2010. *Meteorol Atmos Phys* 129:131–144. <https://doi.org/10.1007/s00703-016-0462-0>
- Ongoma V, Chen H, Gao C (2018) Projected changes in mean rainfall and temperature over East Africa based on CMIP5 models. *Int J Climatol* 38(3):1375–1392. <https://doi.org/10.1002/joc.5252>
- O'Neill BC et al (2017) The roads ahead: narratives for shared socioeconomic pathways describing world futures in the 21st century. *Glob Environ Change* 42:169–180. <https://doi.org/10.1016/j.gloenvcha.2015.01.004>
- Onyutha C (2020) Analyses of rainfall extremes in East Africa based on observations from rain gauges and climate change simulations by CORDEX RCMs. *Clim Dyn* 54:4841–4864. <https://doi.org/10.1007/s00382-020-05264-9>
- Onyutha C (2019) African food insecurity in a changing climate: the roles of science and policy. *Food Energy Sec* 8(1):e00160. <https://doi.org/10.1002/fes3.160>
- Onyutha C (2021) Trends and variability of temperature and evaporation over the African continent: relationships with precipitation. *Atmósfera* 34(3):267–287. <https://doi.org/10.20937/atm.52788>
- Palmer PI, Wainwright CM, Dong B, Maidment RI, Wheeler KG, Gedney N, ... Turner AG (2023) Drivers and impacts of Eastern African rainfall variability. *Nat Rev Earth Environ* 4(4): 254–270. <https://doi.org/10.1038/s43017-023-00397-x>
- Pendergrass AG, Meehl GA, Pulwarty R, Hobbins M, Hoell A, AghaKouchak A et al (2020) Flash droughts present a new challenge for subseasonal-to-seasonal prediction. *Nat Clim Change* 10(3):191–199. <https://doi.org/10.1038/s41558-020-0709-0>
- Parhi P, Giannini A, Gentine P, Lall U (2016) Resolving contrasting regional rainfall responses to El Niño over tropical Africa. *J Clim* 29(4):1461–1476. <https://doi.org/10.1175/JCLI-D-15-0071.1>
- Sanderson BM, Wehner M, Knutti R (2017) Skill and independence weighting for multi-model assessments. *Geosci Model Dev* 10(6):2379–2395. <https://doi.org/10.5194/gmd-10-2379-2017>
- Soccimarro E, Gualdi S (2020) Heavy daily precipitation events in the CMIP6 worst-case scenario: projected twenty-first-century changes. *J Clim* 33(17):7631–7642. <https://doi.org/10.1175/JCLI-D-19-0940.1>
- Seneviratne SI, Nicholls N, Easterling D, Goodess CM, Kanae S, Kossin J et al (2012) chapter 3- Changes in climate extremes and their impacts on the natural physical environment. In: Field CB, Barros V, Stocker TF, Qin D, Dokken DJ, Ebi KL, Mastrandrea MD, Mach KJ, Plattner G-K, Allen SK, Tignor M, and Midgley PM (eds) Managing the risks of extreme events and disasters to advance climate change adaptation. A special report of working groups I and II of the Intergovernmental


- Panel on Climate Change (IPCC). Cambridge University Press, pp 109–230. <https://doi.org/10.1017/CBO9781139177245.006>
- Song YH, Chung ES, Shahid S (2021) Spatiotemporal differences and uncertainties in projections of precipitation and temperature in South Korea from CMIP6 and CMIP5 GCMs. *Int J Climatol* 41:5899–5919. <https://doi.org/10.1002/joc.7159>
- Sun X, Ge F, Chen Q, Fraedrich K, Li X (2023) How striking is the intergenerational difference in exposure to compound heatwaves over Southeast Asia? *Earth's Future* 11(6):e2022EF003179. <https://doi.org/10.1029/2022EF003179>
- Tabari H, Willems P (2023) Global risk assessment of compound hot-dry events in the context of future climate change and socioeconomic factors. *npj Clim Atmos Sci* 6(1):74. <https://doi.org/10.1038/s41612-023-00401-7>
- Taylor KE (2001) Summarizing multiple aspects of model performance in a single diagram. *J Geophys Res* 106:7183–7192. <https://doi.org/10.1029/2000JD900719>
- Tierney JE, Ummenhofer CC, DeMenocal PB (2015) Past and future rainfall in the horn of Africa. *Sci Adv* 1:e1500682. <https://doi.org/10.1126/sciadv.1500682>
- Ullah S, You Q, Chen D, Sachindra DA, AghaKouchak A, Kang S et al (2022) Future population exposure to daytime and nighttime heat waves in South Asia. *Earth's Future* 10(5):e2021EF002511. <https://doi.org/10.1029/2021ef002511>
- Ullah I, Saleem F, Iyakaremye V, Yin J, Ma X, Syed S et al (2022a) Projected changes in socioeconomic exposure to heatwaves in South Asia under changing climate. *Earth's Future* 10: e2021EF002240. <https://doi.org/10.1029/2021EF002240>
- Ullah I, Ma X, Asfaw TG, Yin J, Iyakaremye V, Saleem F et al (2022b) Projected changes in increased drought risks over South Asia under a warmer climate. *Earth's Future* 10: e2022EF002830. <https://doi.org/10.1029/2022EF002830>
- Ullah I, Zeng XM, Mukherjee S, Aadhar S, Mishra AK, Syed S, Ayugi BO, Iyakaremye V, Lv H (2023) Future amplification of multivariate risk of compound drought and heatwave events on South Asian population. *Earth's Future* 11(12):e2023EF003688. <https://doi.org/10.1029/2023EF003688>
- Ullah I, Mukherjee S, Syed S et al (2024) Anthropogenic and atmospheric variability intensifies flash drought episodes in South Asia. *Commun Earth Environ* 5:267. <https://doi.org/10.1038/s43247-024-01390-y>
- Wang Y, Yuan X (2021) Anthropogenic speeding up of South China flash droughts as exemplified by the 2019 summer-autumn transition season. *Geophys Res Lett* 48(9):1–9. <https://doi.org/10.1029/2020GL091901>
- Weber T, Bowyer P, Rechid D, Pfeifer S, Raffaele F, Remedio AR ... Jacob D (2020) Analysis of compound-climate extremes and exposed population in Africa under two different emission scenarios. *Earth's Future* 8(9):e2019EF001473. <https://doi.org/10.1029/2019EF001473>
- Wu Y, Miao C, Sun Y, AghaKouchak A, Shen C, Fan X (2021) Global observations and CMIP6 simulations of compound extremes of monthly temperature and precipitation. *GeoHealth* 5(5):e2021GH000390. <https://doi.org/10.1029/2021GH000390>
- Zhao C, Feng Y, Wang T, Liu W, Wang H, Liu Y, Sun F (2023) Projected changes in socioeconomic exposure to compound hot–dry/hot–wet days in China under CMIP6 forcing scenarios. *Theor Appl Climatol* 1–12. <https://doi.org/10.1007/s00704-023-04575-1>
- Zhang G, Wang H, Gan TY, Zhang S, Shi L, Zhao J et al (2022) Climate change determines future population exposure to summertime compound dry and hot events. *Earth's Future* 10: e2022EF003015. <https://doi.org/10.1029/2022EF003015>
- Zhang X, Gu X, Slater LJ, Dembélé M, Tosunoğlu F, Guan Y, Liu J, Zhang X, Kong D, Xie F, Tang X (2023) Amplification of coupled hot-dry extremes over Eastern Monsoon China. *Earth's Future* 11(12):e2023EF003604. <https://doi.org/10.1029/2023EF003604>
- Zhang W, Luo M, Gao S, Chen W, Hari V, Khouakhi A (2021) Compound hydrometeorological extremes: drivers, mechanisms and methods. *Front Earth Sci* 9(October):1–20. <https://doi.org/10.3389/feart.2021.673495>
- Zhou S, Yu B, Zhang Y (2023) Global concurrent climate extremes exacerbated by anthropogenic climate change. *Sci Adv* 9(10):eabo1638. <https://doi.org/10.1126/sciadv.abo1638>
- Zhu H, Jiang Z, Li L (2021) Projection of climate extremes in China, an incremental exercise from CMIP5 to CMIP6. *Sci Bull* 66:2528–2537. <https://doi.org/10.1016/j.scib.2021.07.026>

- Zhu HH, Jiang S, Jiang ZH (2022) Projection of climate extremes over China in response to 1.5/2°C global warming based on the reliability ensemble averaging (in Chinese). *Adv Earth Sci* 37:612–626. <https://doi.org/10.11867/j.issn.1001-8166.2022.028>
- Zhu H, Jiang Z, Li L, Li W, Jiang S, Zhou P, ... Li T (2023) Intercomparison of multi-model ensemble-processing strategies within a consistent framework for climate projection in China. *Sci China Earth Sci* 66(9): 2125–2141. <https://doi.org/10.1007/s11430-022-1154-7>
- Zscheischler J, Seneviratne SI (2017) Dependence of drivers affects risks associated with compound events. *Sci Adv* 3(6):e1700263. <https://doi.org/10.1126/sciadv.1700263>

Publisher's Note Springer Nature remains neutral with regard to jurisdictional claims in published maps and institutional affiliations.

Springer Nature or its licensor (e.g. a society or other partner) holds exclusive rights to this article under a publishing agreement with the author(s) or other rightsholder(s); author self-archiving of the accepted manuscript version of this article is solely governed by the terms of such publishing agreement and applicable law.

Authors and Affiliations

Brian Odhiambo Ayugi¹ · Charles Onyutha² · Kenny Thiam Choy Lim Kam Sian³ · Huanhuan Zhu³ · Hassen Babousmail³ · Eun-Sung Chung¹ 

✉ Eun-Sung Chung
eschung@seoultech.ac.kr

¹ Faculty of Civil Engineering, Seoul National University of Science and Technology, 232 Gongneung-Ro, Nowon-Gu, Seoul 01811, South Korea

² Department of Civil and Environmental Engineering, Kyambogo University, P.O. Box 1, Kyambogo, Kampala, Uganda

³ School of Atmospheric Science and Remote Sensing, Wuxi University, Wuxi 214105, China